Journal Name

ARTICLE TYPE

Cite this: DOI: 10.1039/xxxxxxxxxx

Tuning ultrafast electron injection dynamics at the organic-graphene/metal interface†

Abhilash Ravikumar,[‡a] Gregor Kladnik,[b,c] Moritz Müller,[d] Albano Cossaro,[e] Gregor Bavdek,[f] Laerte L Patera,[c,e] Daniel Sánchez Portal,[d] Latha Venkataraman,[g,h] Alberto Morgante,[c,e] Gian Paolo Brivio,[a] Dean Cvetko,[◇b,e,i] and Guido Fratesi*[j]

Received Date
Accepted Date

DOI: 10.1039/xxxxxxxxxx

www.rsc.org/journalname

We compare the ultrafast charge transfer dynamics from molecules on epitaxial graphene and bilayer graphene grown on Ni(111) interfaces through first principle calculations and x-ray resonant photoemission spectroscopy. We use 4,4′-bipyridine as the prototypical molecule for these explorations as the energy level alignment of core-excited molecular orbitals allows ultrafast injection of electrons from the substrate to the molecule on a femtosecond timescale. We show that the ultrafast injection of electrons from the substrate to the molecule is almost an order of magnitude faster on epitaxial graphene when compared to the bilayer substrate. Through our experiments and calculations, we can attribute this to the difference in the density of states close to Fermi level between graphene and bilayer graphene. We therefore show how the electronic structure of the substrate influences charge transfer dynamics between organic molecules and graphene interfaces.

Graphene, a two-dimensional allotrope of carbon with a honeycomb lattice geometry, has inspired a lot of research interest since its discovery in 2004[1–4]. It's use as an ultra thin, quasi-transparent electrode for photovoltaics or as charge carrier separator in organic photovoltaics devices[5,6] has been extensively pursued. In this context, the electronic coupling across the hybrid graphene/organic interface plays a crucial role in controlling the functionality and efficiency of such graphene based organic electronic and photovoltaic devices[7–9]. Typically, in these devices, it is important to understand charge transfer from electronically or optically excited molecules; this involves charge injection to or from the unoccupied levels on the molecule to the substrate. A variety of experimental techniques have been proposed to probe the unoccupied energy levels and study the charge transfer dynamics at such hybrid interfaces. These include core-hole-clock (CHC) spectroscopy[7,10,11], two-photon photoemission spectroscopy[12,13], inverse photoemission spectroscopy[14] and time resolved pump-probe methods[15,16]. Here, we focus on core-hole-clock spectroscopy, as it has been used successfully address charge transfer dynamics at organic molecules on metals[7,17–22], semiconductors[23,24] as well as in organic assemblies[25–29].

To compare our experimental results with calculations, we utilize density functional theory (DFT) with a Green's function approach where a substrate (graphene or bilayer graphene on Ni(111)) is coupled to the bulk continuum via self-energy operators. Resonant charge transfer lifetimes are then extracted based on the coupling of the molecular states with those of the substrate[30–32]. This method goes beyond those[33–36] that rely on a finite cluster or slab which typically do not truly capture the nuances of the elastic lifetime without introducing artificial confinement effects in the electronic structure.

In this work we study the charge transfer dynamics of a weakly molecule, 4,4′-bipyridine ($C_5H_4N_2$, BP), adsorbed on epitaxial graphene grown on Ni(111) and bilayer graphene on Ni(111). We determine charge transfer times by core-hole-clock spectroscopy, photoexciting N 1s core electrons to unoccupied molecular orbitals or to unbound states and determining the decay path-

[a] Dipartimento di Scienza dei Materiali, Università di Milano-Bicocca, Via Cozzi 55 - 20125 Milano, Italy. Fax:+39-02-644854000; Tel: +393451475855
[b] Faculty for mathematics and physics, University of Ljubljana, Slovenia
[c] Dipartimento di Fisica, Università di Trieste, Italy
[d] Centro de Física de Materiales and Donostia International Physics Center, Paseo Manuel de Lardizabal 5, 20018 San Sebastián, Spain
[e] CNR-IOM Laboratorio Nazionale TASC, Trieste, Italy
[f] Faculty of education, University of Ljubljana, Ljubljana, Slovenia
[g] Dept. of Applied Physics and Applied Mathematics, Columbia University, New York
[h] Dept. of Chemistry, Columbia University, New York
[i] Institut J. Stefan, Janova 39, Ljubljana, Slovenia
[j] Dipartimento di Fisica, Università degli Studi di Milano, Via Celoria, 16 - 20133 Milano, Italy

† Electronic Supplementary Information (ESI) available: [details of any supplementary information available should be included here]. See DOI: 10.1039/b000000x/

E-mail of Corresponding authors-
‡: a.ravikumar@campus.unimib.it
◇ : dean.cvetko@fmf.uni-lj.si
∗ : guido.fratesi@unimi.it

ways of this excited state. We compare these experimental results with our DFT calculations employing non-equilibrium Green's function techniques. We find that the timescale for ultrafast electron injection from graphene to core-excited molecules increases by about one order of magnitude from epitaxial graphene to bilayer graphene. This trend is reproduced by the calculations that highlight the role of graphene/Ni(111) coupling on the charge transport properties at the above organic-graphene interface.

Methods

Simulation Details

The calculations are performed within the SIESTA/TranSIESTA[37,38] quantum transport package and parallel molecular break-junction simulations[39], as introduced previously[30,32]. We setup the system as a 6×6 supercell periodic in the surface x-y plane, as shown in Fig. 1(a). The surface region, coupled in the z direction to an infinitely extended Ni(111) crystal ("electrode"), is constituted of bipyridine adsorbed on either epitaxial graphene/nickel (BP/EG/Ni) or bilayer graphene/nickel (BP/BLG/Ni), as shown in Fig. 1(b) and (c), including 7 and 4 Ni layers, respectively. We assume a close epitaxial matching of graphene lattice with that of the Ni(111) surface, given the small lattice mismatch of free-standing graphene with nickel (less than 1.5 %, with a lattice constant of 2.51 Å in agreement with previous calculations[40]). Following previous studies of graphene on Ni(111)[41–45], we modeled EG/Ni in the atop/fcc-hollow configuration, where the nomenclature refers to the position of the C atoms with respect to the underlying Ni sites. For BLG/Ni, a top graphene layer was added with C atoms stacked in the AB configuration of graphite. The top layer of graphene is in the hollow configuration with respect to the nickel substrate.

We adopted a fully non-local van der Waals exchange-correlation functional as proposed by Klimes, Bowler and Michaelides (vdW-KBM)[46] with a real space grid cutoff of 300 Ry. A localized basis set consisting of double-ζ polarized orbitals is used for all the atoms in the system. A Γ-centered Monkhorst-Pack k-point mesh corresponding to a 36×36 mesh in the 1×1 Ni(111) unit cell is used to sample the surface Brillouin zone. Given the fairly large unit cells and the dispersive nature of the interaction with graphene, the adsorption site of bipyridine is chosen on the basis of our analysis for the molecule on free standing graphene (BP/FSG), leading to a configuration of the molecule with the two N atoms above a graphene atom and at the center of a graphene hexagon (see SI for further details[47]). This is further optimized in a standard slab calculation with SIESTA for BP/EG/Ni and BP/BLG/Ni with results shown in Fig. 1(b) and (c), respectively. An average molecule-graphene distance of BP/EG/Ni is 3.04 Å (3.06 Å for BP/BLG/Ni) is computed. The molecule flattens upon adsorption reducing the torsional angle between the phenyl rings from a gas phase value of 37°[48] to 11° and 18° for BP/EG/Ni and BP/BLG/Ni respectively. We simulate the core-level excitation by replacing the standard pseudopotential of the excited N atom with one having a full core hole (FCH) in the 1s orbital, and considering a globally neutral system with the positive core balanced by an additional electron in the valence band. This models the final state of x-ray resonant photo-absorption, or of a photoemission experiment where the valence shell relaxes around the core hole by attracting an electron from the substrate reservoir[19,32,49]. Within the Green's function approach to charge transfer dynamics[10,19,32,37], the density of states projected onto a localized molecular state $\phi(\mathbf{r})$ is computed in terms of the Green's function of the surface region as a function of energy E as

$$\rho_\phi(E) = \frac{1}{\pi}\Im\left[\int dr \int dr' \phi^*(\mathbf{r}) G(\mathbf{r},\mathbf{r}',E)\phi(\mathbf{r}')\right]. \qquad (1)$$

The full width at the half maximum (fwhm, Γ) of $\rho_\phi(E)$ finally provides the resonant lifetime $\tau = \hbar/\Gamma$ for an electron (or an hole) initially occupying the state ϕ, that is our estimate for the transfer time to (from) the substrate. Additional details about the system setup in the molecular break junction-like geometry and computational parameters are presented in the SI[47].

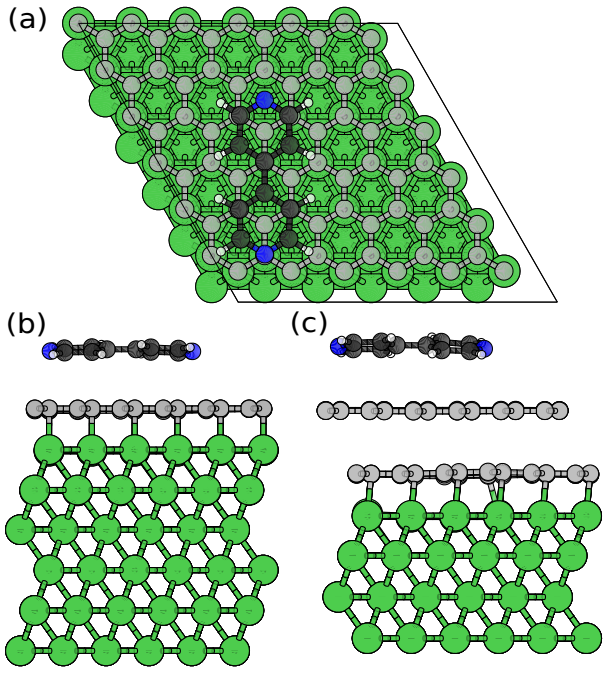

Fig. 1 (a) Top view of the system geometry showing the 6×6 supercell with bipyridine adsorbed on epitaxial graphene/Ni(111) substrate. (b) Side views for the BP/EG/Ni and (c) BP/BLG/Ni. The last three layers of Ni are coupled to a bulk electrode in a molecular break junction-like setup.

Experimental methods

Sample preparation and characterization

Graphene (GR) layers have been prepared under ultra high vacuum (UHV) by Chemical Vapour Deposition (CVD) on a Ni(111) substrate[50] (see SI for details of sample preparation[47]). The Ni(111) and GR/Ni(111) substrates have been characterized by XPS and UV photoemission. All experiments were performed at the ALOISA and HASPES beamlines of the IOM laboratory at Elettra synchrotron in Trieste. GR coupling to the Ni substrate was monitored by angle resolved UV photoemission with He II pho-

ton line at 40.8 eV. Characteristic dispersion of the GR π band along the ΓK and ΓM directions (see SI for details[47]) was used to identify the presence of EG and BLG phases. 4,4' bipyridine molecules were evaporated from a pyrex glass tube, operating at room temperature, to the substrate kept at 220-250 K, obtaining a coverage below the monolayer one. The C1s, N1s, Ni 3p X-ray photoemission was used to check the chemical composition of the BP molecular film. Near edge absorption fine structure (NEXAFS) of C and N K-edges was used in *s-pol* (TM geometry with electric field parallel to the surface) and in *p-pol* (TE geometry with photon electric field normal to the surface) to measure the molecular adsorption geometry through average inclination (tilt) of the BP aromatic system, as detailed in the Supplemental Information[47]. BP/EG/Ni and BP/BLG/Ni monolayer films display a very strong and almost identical linear dichroism of the transition from N1s to the lowest unoccupied molecular orbital (LUMO), from which an almost flat lying adsorption geometry at an average angle of 16° (BP/EG/Ni) and 20±3° (BP/BLG/Ni) can be deduced, taking into account both tilt and twist of the molecule. These are in good agreement with theoretical values of 11° and 18°, respectively.

Resonant photoemission

Resonant photoemission was performed as a series of photoemission spectra across the nitrogen (carbon) K-edge with the photon energy tuned in steps of 0.1 eV through the N1s (C1s) absorption edge at $395-415$ eV ($284-310$ eV). The photon was incident at 4° and the photon polarization was set perpendicular to the surface (TM geometry, p-pol). The electron analyzer was aligned with the sample normal and photon polarization. At each photon energy, single photoemission spectra were measured in a wide binding energy range (60 eV$< E_B < -2$ eV) relative to the Fermi energy. All spectra have been merged in a false color RPES maps represented in kinetic energy scale $I(h\nu, E_k)$.

Results and discussion

Ground state properties

We start by examining the two different graphene systems; the epitaxial graphene with strong electronic coupling to the Ni(111) substrate and the bilayer graphene, where the outermost graphene layer is effectively decoupled from the substrate beneath, thus closely resembling that of a freestanding graphene[51]. This electronic decoupling of graphene layers can be appreciated by examining the density of states (DOS) of these systems. The strong hybridization of EG with the states of nickel breaks the symmetry and opens a bandgap in graphene at the K-point[52]. A large density of states of graphene appears close to the Fermi level of Ni as can be seen in Fig. 2(a) where the DOS of bulk Ni and the graphene projections of 1×1 EG/Ni are plotted. Figure 2(c) shows instead the graphene projections of 1×1 BLG/Ni, separating the two layers of graphene. While the topmost layer (red curve) remains fairly decoupled from the substrate[51], the bottom layer in contact with Ni (black curve) shows a remarkable modification in close analogy to the results of EG/Ni that we show in Fig. 2(a). Figure 2(e) shows the DOS of pristine graphene for reference. This gives us a clear contrast in the electronic coupling that BP would experience upon adsorption.

The experimental aspect of the modification of the graphene electronic structure in both systems is evidenced by the valence band structure measured by angle resolved UV photoemission. We refer to the SI for details[47] regarding the experimental setup and comment here on the UV spectra at normal emission that are presented in Fig. 3(a). The signal detected for bilayer graphene is predominantly from the top most layer of graphene, whose weak coupling can be appreciated from the resulting π band which shows a dispersion character very similar to free standing graphene[47], with band bottom at Γ point reaching a binding energy of -8.5 eV, in agreement with Ref.[53]. The more strongly coupled EG phase, on the other hand shows π band shifted to lower binding energies with band bottom at Γ point reaching -10.5 eV[54,55] due to the stronger hybridization of graphene with the Ni(111) substrate.

When BP is adsorbed on EG/Ni or BLG/Ni, the electronic DOS of the graphene layers is minimally altered due to the dominant dispersion character of the interaction. From the BP point of view, the weak interaction is reflected in well-defined peaks in the molecular-projected DOS of the full system, that is computed by projecting on the individual molecular orbitals of gas phase BP and is reported as unshaded curves in Fig. 2(b), (d), and (f) for BP/EG/Ni, BP/BLG/Ni and BP/FSG, respectively. By comparing the molecular DOS on BLG/Ni and FSG to that on EG/Ni, the main observation is a shift of the orbitals towards lower binding energies, that is practically orbital-independent and that amounts to about 0.75 eV for BLG and 0.70 eV for FSG. This shift equals a change of the graphene/substrate work function that we compute to increase from EG/Ni to BLG/Ni by 0.7 eV (see the SI for details about these results[47]). At a finer level, one can also appreciate a decrease in the coupling of the LUMO orbital as evidenced by its width, i.e., $\Gamma = 161$ meV, 89 meV, and 31 meV, for the LUMO of BP on EG, BLG, and FSG, respectively. That however is less system-dependent that in the core-excited case (see below). Remarkably, none of the three cases presents a significant molecular spin polarization in the ground state despite the spin-polarized substrate.

The relative independence of the molecular electronic structure on the specific graphene layer underneath, apart for an energy level offset, is also demonstrated by core-level photoemission and valence band photoemission techniques. Figure 3(b) shows the C1s and N1s x-ray photoemission spectra (XPS) for both EG/Ni and BLG/Ni systems, before (lower curves) and after (upper curves) adsorbing the molecules. We find the C1s peak for the EG/Ni (BLG/Ni) phase without molecules at 285 eV (284.6 eV) binding energy. The XPS spectrum of a multilayer BP film, also presented in Fig. 3(b), shows a single N1s peak at 399.8 eV and C1s doublet at 285.6 and 286.4 eV belonging respectively to 4 C atoms next to N ones and to the 6 remaining carbons within the BP molecule. BP/EG/Ni and BP/BLG/Ni spectra (see Fig. 3(b), upper curves) are qualitatively similar to the BP multilayer apart from the rigid shift to lower binding energies. Interestingly, such a shift amounts to 0.4 eV for both N1s and C1s core levels in BP when passing from BP/EG/Ni to BP/BLG/Ni, similar to the C1s shift of the clean EG/Ni and BLG/Ni main peak. These indicate that the modified electronic structure between the EG and BLG

phases is equally reflected in the energy level offset of orbitals in the adsorbed organic layer and could be attributed to a variation of the dipole layer at the graphene-Ni interface.

Electron transfer dynamics

We now study the influence of the variable coupling at the interface on the electron transfer dynamics, using RPES. Figure 4 shows RPES results for BP multilayer (a), BP/EG (b), and BP/BLG (c) represented in the form of intensity color map versus photon energy (vertical axis) and electron kinetic energy (horizontal axis). These maps are constructed from photoemission scans taken at a series of incident photon energies tuned across the nitrogen K absorption edge. To highlight the resonant contribution in the photoemission spectra, the non-resonant component (due to direct photoemission from the BP orbitals and from the substrate) has been measured at $h\nu = 395$ eV (below the resonant edge) and subtracted from all spectra shown in Fig. 4. As the photon energy is set to the excitation of the LUMO resonance ($h\nu \approx 399$ eV, see the red lines), the spectrum is composed by a broad Auger line centered at about $E_k = 385$ eV, and sharper features coinciding with the direct photoemission from the molecular orbitals (HOMO$-n$, $n = 0,1,2,\ldots$). The latter originate from processes named "participator" resonances (P), where the excited electron in the LUMO* state participates in the decay of the core-hole and an Auger electron from the filled molecular orbital is elastically emitted[10] as schematically depicted in Fig. 4(d) for the process involving the HOMO, with $E_k = 394$ eV. They are best seen for BP/EG in Fig. 4(b) where they are marked by gray lines. Note that the single RPES spectra taken at the LUMO resonances (red lines) are quite similar for multilayer and single layer BP, and they resemble non-resonant, direct photoemission spectra of the respective systems. Participator peaks are not expected with $h\nu$ above the ionization threshold, see Fig. 4(a).

Intriguingly, spectral features at the same kinetic energy as the participator peaks may be observed for BP/EG/Ni also for photon energies above the absorption edge[56] when the LUMO state is filled by an electron transferred from the environment to the molecule[19,20], instead of being directly populated by the excitation. These processes are named "superparticipator" decays (SP) and are schematically shown in Fig. 4(d); their constant kinetic energy indicates that an identical core-hole decay process occurs independently of the excitation energy and reflects that LUMO* is occupied in the core excited intermediate state. We average the non-resonant spectra in the energy range from 411 eV to 417 eV (blue lines in Fig. 4) and observe clear SP peaks only observed for the monolayer BP. Their presence reflects ultrafast electron injection from the substrate to the LUMO*, taking place during the ultrashort time window of the core-hole lifetime. Energy alignment of the LUMO* orbital below Fermi level in presence of the core hole is required for this to occur and the relative intensity of the SP peaks is determined by the probability of LUMO* filling and the relevant timescale for the substrate electron injection to the LUMO*. By assuming equal timescale for electron injection to / delocalization from the LUMO*, and analyzing the intensity of the SP and P peaks of BP/EG/Ni relative to the P intensity of the multilayer BP, as detailed in[19], we can quantify the charge injection time of $\tau_{EG} = 4 \pm 1$ fs[20]. The energy diagram of the SP decay process involving electron injection from the substrate is schematically shown in Fig. 4(d).

The RPES maps of BP/BLG/Ni, shown in Fig. 4(c), present an intermediate case between multilayer and BP/EG/Ni: superparticipator lines above the ionization edge are observed on BLG, but significantly attenuated than those for EG. Here the relative intensity of the SP and P peaks may be converted to the electron injection time $\tau_{BLG} = 30 \pm 5$ fs. This indicates that the electron transfer at the organic/graphene interface is strongly slowed down for the poorly interacting graphene/Ni layers. A similar ratio, up to a factor 6, was measured for electron transfer from Ar atoms to graphene on various substrates as the coupling was reduced[57].

To compare these measurements with theoretical findings, we need to include the influence of the core-hole in the simulation as this is fundamental for the alignment of the molecular energy around the Fermi level and its filling. To this purpose, the total DOS of the N1s-excited systems projected on the molecular orbitals of bipyridine, are plotted in Fig. 2(b) and (d) for BP/EG/Ni and BP/BLG/Ni, respectively. Upon core excitation at the N1s edge, the molecular states move to lower energies due to the attractive potential generated by the positive core hole and charge populates the molecular region to screen its perturbation. The valence of the system relaxes around the core hole and the additional electron now mostly populates the spin-majority LUMO* of the molecule, that needs to shift below the Fermi level to accommodate such charge. This leads to a magnetic moment of the valence electrons of 1 μ_B on the molecule that remains spin polarized until the core hole de-excites back via one of several decay channels or the electron is transferred to graphene[58]. The other molecular orbitals are also shifted in energy but their precise position (which would instead require a many body approach for a proper determination) is not relevant for our discussion. We describe similarly the case where the LUMO* is directly populated (in the resonance condition) and that where $h\nu$ is above the ionization threshold: in the latter, the core-level excitation calls for electron transfer from the substrate eventually producing the superparticipator decay channels. The computed width of the LUMO* in the DOS allows us the estimate the relevant timescale related to P and SP decays, respectively.

Visual inspection of Fig. 2(b) and (d) already testifies that, for the BP/BLG/Ni case, the LUMO* appears to decouple from the substrate states and the peak becomes narrower than in BP/EG/Ni. Indeed, its intrinsic width Γ amounts to 6 meV (20 meV) for BP/BLG/Ni (BP/EG/Ni) and a corresponding resonant lifetime of ~ 116 fs (~ 33 fs). Although numerical times are somehow overestimated at this simple level of theory, where no dynamical effect is explicitly considered (in agreement with estimates for other systems[19,32]), the experimental trend is nicely reproduced and is now analyzed further in terms of the calculated electronic properties. We recall that the layer of graphene in contact with the nickel substrate shows large graphene states close to the Fermi level but a second graphene layer, which is interacting with the molecule in BP/BLG/Ni, bears close resemblance to pristine graphene with very few states close to the Fermi level. Hence

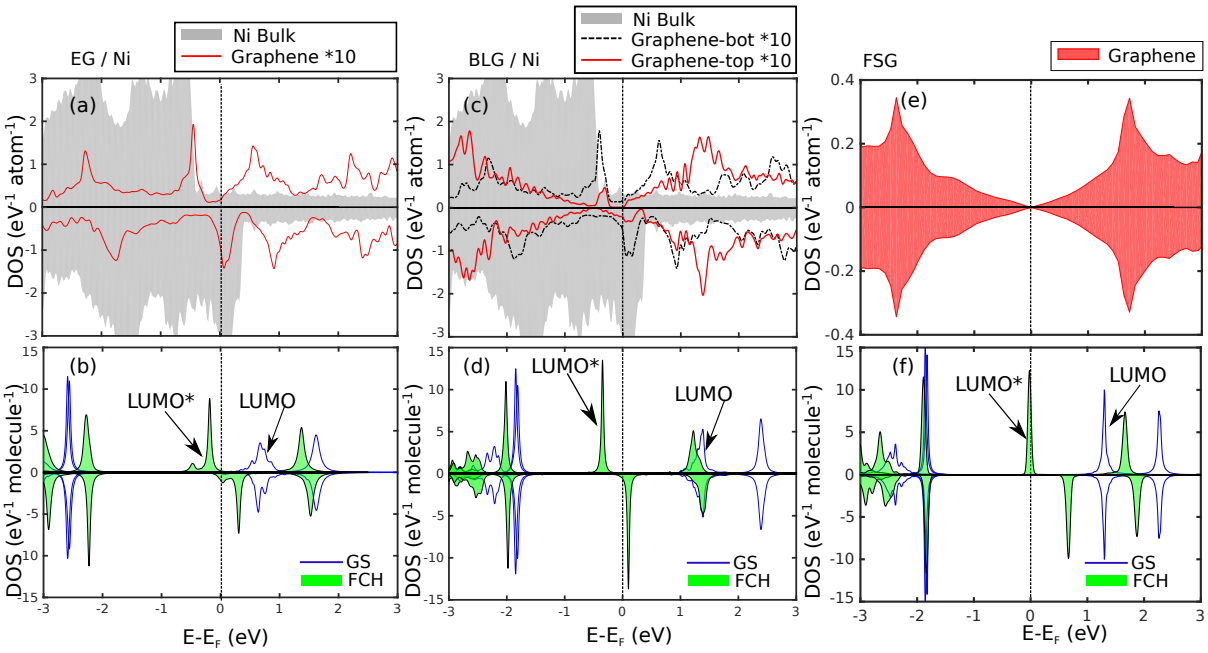

Fig. 2 (a) The bulk DOS of Ni and DOS of 1×1 EG/Ni projected onto the orbitals of graphene. (b) The total DOS of BP/EG/Ni projected onto the molecular orbitals of bipyridine in the ground state (GS) and core excited one (FCH). (c) The bulk DOS of Ni and DOS of 1×1 BLG/Ni projected onto the orbitals of bilayer graphene. (d) Same as (b) for BP/BLG/Ni. (e) The DOS of free standing graphene and (f) molecular projections of bipyridine/free standing graphene. The Ni and graphene DOS are plotted with a Gaussian broadening of 0.04 eV; molecular projections include instead a Lorentzian broadening of 0.04 eV. Positive/negative values are used for spin majority/minority DOSs.

the coupling of the LUMO* to substrate states is significantly suppressed.

Information about the charge transfer can be gained by the local density of states corresponding to states with energies around the LUMO* of bipyridine. That is plotted in Fig. 5. In both cases, this quantity in the molecular region exhibits the shape and symmetry of the LUMO of gas phase BP (the LUMO of BP in the gas phase, and other frontier molecular orbitals, are depicted in the SI[47]) with amplification of the amplitude towards the core excited atom. A similar amount of states is present in the layer of graphene in contact with Ni. However, a clear distinction between EG and BLG cases is the charge density on the layer of graphene in contact with the molecule, as visible by comparing Fig. 5 (a) and (b). We see that for BP/BLG/Ni case, the LUMO*, which upon excitation shifts close to the Fermi level, finds very few states of the top layer of graphene to couple with, unlike the case of BP/EG/Ni.

So far we have theoretically considered resonant transfer from a LUMO state populated by an electron belonging to the majority spin population, corresponding to resonant absorption of a core electron with the same spin, or to photoemission and subsequent electron transfer. However, a resonant excitation could also involve a minority spin electron, which would couple resonantly to substrate states with the same spin. This case also deserves our attention. Since filling of the spin-minority LUMO* does not correspond to the electronic ground state (optimized with the N1s* atom) accessible to simulations, this is modeled by a post-self-consistent method described in the SI[47]. Similarly to the results reported above for the spin-majority population, for the spin-minority LUMO* we calculate a remarkable slowing down for the electron transfer processes in BP/BLG/Ni ($\Gamma = 5$ meV, $\tau = 120$ fs) with respect to BP/EG/Ni ($\Gamma = 36$ meV, $\tau = 19$ fs). Interestingly, BP/EG/Ni presents a moderate spin-dependence of the fwhm that can be ascribed to the higher DOS of Ni in the minority spin channel around the Fermi energy; conversely, practically no dependence is found for BP/BLG/Ni where the metal substrate is more effectively screened by the two graphene layers.

The limiting case of a fully uncoupled C layer is represented by bipyridine adsorbed on pristine graphene, that we present to further clarify the above results. Here, due to the unique DOS of graphene with the presence of the Dirac cone at the Fermi level (and therefore the absence of substrate states at the Fermi level) as seen in Fig. 2(e), the theoretical modeling predicts a completely uncoupled LUMO* upon core excitation with an infinite resonant lifetime. As seen in Fig. 2(f), molecular states of bipyridine on pristine graphene in the ground state have very similar energies to BP/BLG/Ni case shown in Fig. 2(b). Due to the weak interaction of the molecule with graphene, the Dirac point is not significantly perturbed by adsorption. But upon photoemission of a core level electron and complete relaxation of the valence shell, the molecular orbitals move to lower energies as seen in the previous cases, with a spin-majority LUMO* mostly below the Fermi level to accommodate an additional electron. The LUMO* now encounters the Dirac point of graphene where no states are found, so it completely decouples from the substrate producing, in principle an infinitely sharp state with $\tau = \infty$ (this hypothetical picture is only approximately reproduced in actual simulations because of finite size of the surface unit cell). Clearly, this neglects all dy-

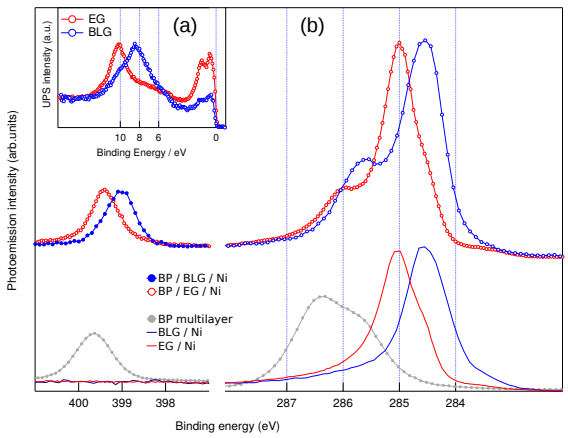

Fig. 3 (a) Normal emission valence band photoemission spectra with photon energy of 40.8 eV for EG/Ni and BLG/Ni phases. The π band peak at Γ point is evidenced at 10.5 and 8.5 eV binding energy, respectively. Ni band features may be seen in a 2 eV energy window below the Fermi level (set at 0 eV), with significantly stronger attenuation due to inelastic scattering in the BLG phase. (b) Lower curves: Carbon 1s XPS with photon energy of 500 eV from bare EG/Ni (red curve) and BLG/Ni (blue curve), as well as N1s and C1s XPS from bipyridine multilayer (black markers). Upper curves: N1s and C1s XPS of bipyridine monolayer on EG (BP/EG/Ni, red markers) and BLG (BP/BLG/Ni, blue markers).

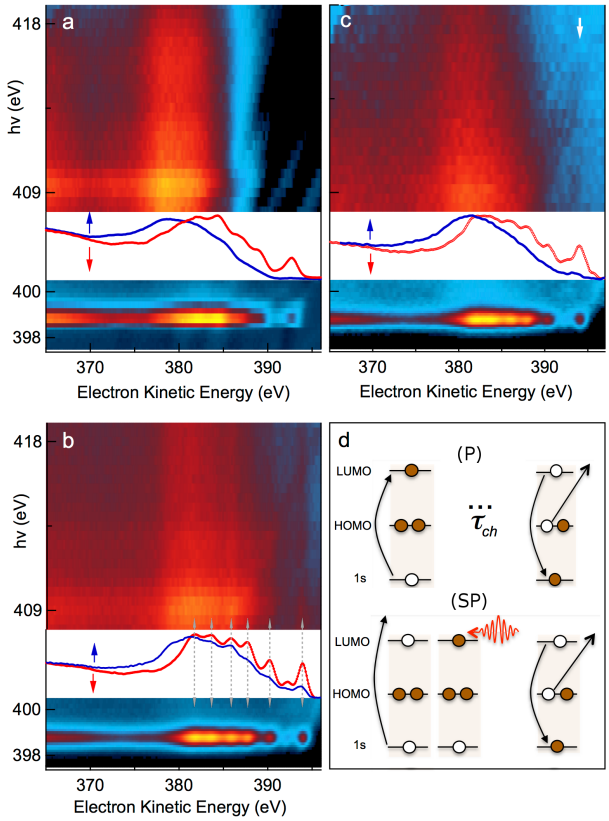

Fig. 4 (a) Nitrogen K-edge RPES map for BP multilayer, (b) monolayer BP/EG and (c) BP/BLG . Each graph shows separately RPES around the N1s $\rightarrow$LUMO* resonance (lower sub-panel, $h\nu \sim 399$ eV) and above the excitation edge (upper sub-panel). Direct comparison of the resonant ($h\nu \sim 399$ eV, red lines) and non-resonant spectra (averaged in the photon energy range 411 eV $< h\nu <$ 417 eV, blue lines) are also shown in the middle sub-panels. The energy level diagram of the participator (P) and superparticipator (SP) processes, whose energies are marked by gray lines in panel (b), are illustrated in panel (d).

namical effects in evaluating Kohn Sham eigenvalues for the final state time-independent Hamiltonian, as well as phononic perturbation and lattice defects that would influence a measured lifetime, yielding to the overestimated theoretical value.

Conclusions

Through DFT calculations and x-ray resonant photoemission spectroscopy measurements, we have shown that charge injection from graphene/Ni(111) in an adsorbed organic molecule is an order of magnitude more efficient than from bilayer graphene. We can attribute the difference in the injection rate to the strong electronic coupling of graphene to the underlying Ni substrate. In contrast, the second layer in a bilayer film is weakly coupled to the Ni(111) making its charge injection ability closer to those of free standing graphene. Our work, taken together demonstrates that intercalated graphene effectively decouples organic molecule/graphene interfaces also in terms of electron transfer times.

Acknowledgement

This project has received funding from the European Union Seventh Framework Programme under grant agreement no. 607232 [THINFACE] and A.R. and M.M. are grateful for this. The work is performed within the PCAM European doctorate. G.K. and D.C. acknowledge support from the Slovenian Research Agency (P1-0112). A.C. acknowledges support from the ANCHOR project of the MIUR FIRB 2010. M.M. and D.S.P. acknowledge partial support from MINECO MAT2016-78293-C6-4-R. Support from MIUR (PRIN 20105ZZTSE) and MAE (US14GR12) is acknowledged.

Author contributions statement

The research was designed and directed by G.F. and D.C.. A.R. performed the numerical simulations, assisted by M.M. and D.S.P. and guided by G.P.B. and G.F.. D.C., G.K., A.M., A.C., and L.V. designed and performed the experiments. Core-hole-clock experiments were analyzed by D.C. and G.K.. G.B., G.K., D.C., and L.P. prepared the graphene samples. A.R., G.F., and D.C., prepared the figures and wrote the paper, together with G.P.B., A.M., and L.V.. All authors jointly discussed the experimental and theoretical results.

Conflict of interests

The authors declare no competing conflict of interests.

References

1 K. S. Novoselov, A. K. Geim, S. V. Morozov, D. Jiang, Y. Zhang, S. V. Dubonos, I. V. Grigorieva and A. A. Firsov, *Science*, 2004, **306**, 666–669.

2 J. C. Meyer, a. K. Geim, M. I. Katsnelson, K. S. Novoselov, T. J. Booth and S. Roth, *Nature*, 2007, **446**, 60–63.

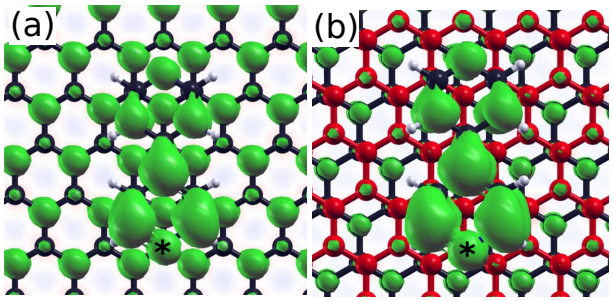

Fig. 5 The local density of states averaged around the LUMO* energy for (a) BP/EG/Ni and (b) BP/BLG/Ni with an isovalue of $0.00167 e Å^{-3} eV^{-1}$. The excited N atom is marked by a star.

3 a. K. Geim, *Science*, 2009, **324**, 1530–1534.

4 a. H. Castro Neto, N. M. R. Peres, K. S. Novoselov, a. K. Geim, F. Guinea and A. Neto, *Reviews of Modern Physics*, 2009, **81**, 109–162.

5 X. Wang, L. Zhi and K. Müllen, *Nano Letters*, 2008, **8**, 323–327.

6 J. Durantini, P. P. Boix, M. Gervaldo, G. M. Morales, L. Otero, J. Bisquert and E. M. Barea, *Journal of Electroanalytical Chemistry*, 2012, **683**, 43 – 46.

7 L. Cao, X.-Y. Gao, A. T. S. Wee and D.-C. Qi, *Advanced Materials*, 2014, **26**, 7880–7888.

8 H. Zhang, X. Lv, Y. Li, Y. Wang and J. Li, *ACS Nano*, 2010, **4**, 380–386.

9 L. Gomez De Arco, Y. Zhang, C. W. Schlenker, K. Ryu, M. E. Thompson and C. Zhou, *ACS Nano*, 2010, **4**, 2865–2873.

10 P. A. Brühwiler, O. Karis and N. Mårtensson, *Reviews of Modern Physics*, 2002, **74**, 703–740.

11 D. Menzel, *Chemical Society Reviews*, 2008, **37**, 2212.

12 H. Ueba and B. Gumhalter, *Progress in Surface Science*, 2007, **82**, 193–223.

13 H. Petek and S. Ogawa, *Progress in Surface Science*, 1997, **56**, 239–310.

14 N. V. Smith, *Reports on Progress in Physics*, 1988, **51**, 1227–1294.

15 X.-Y. Zhu, *The Journal of Physical Chemistry B*, 2004, **108**, 8778–8793.

16 X. Zhu, *Surface Science Reports*, 2004, **56**, 1–83.

17 P. Vilmercati, D. Cvetko, A. Cossaro and A. Morgante, *Surface Science*, 2009, **603**, 1542–1556.

18 G. Kladnik, D. Cvetko, A. Batra, M. Dell'Angela, A. Cossaro, M. Kamenetska, L. Venkataraman, A. Morgante, M. Dell'Angela, A. Cossaro, M. Kamenetska, L. Venkataraman and A. Morgante, *Journal of Physical Chemistry C*, 2013, **117**, 16477–16482.

19 D. Cvetko, G. Fratesi, G. Kladnik, A. Cossaro, G. P. Brivio, L. Venkataraman and A. Morgante, *Phys. Chem. Chem. Phys.*, 2016, **18**, 22140–22145.

20 O. Adak, G. Kladnik, G. Bavdek, A. Cossaro, A. Morgante, D. Cvetko and L. Venkataraman, *Nano Letters*, 2015, **15**, 8316–8321.

21 D. Toffoli, M. Stredansky, Z. Feng, G. Balducci, S. Furlan, M. Stener, H. Ustunel, D. Cvetko, G. Kladnik, A. Morgante, A. Verdini, C. Dri, G. Comelli, G. Fronzoni and A. Cossaro, *Chem. Sci.*, 2017, **8**, 3789–3798.

22 L. Cao, Y.-Z. Wang, T.-X. Chen, W.-H. Zhang, X.-J. Yu, K. Ibrahim, J.-O. Wang, H.-J. Qian, F.-Q. Xu, D.-C. Qi and A. T. S. Wee, *The Journal of Chemical Physics*, 2011, **135**, 174701.

23 J. Schnadt, P. A. Brühwiler, L. Patthey, J. N. O'Shea, S. Södergren, M. Odelius, R. Ahuja, O. Karis, M. Bässler, P. Persson, H. Siegbahn, S. Lunell and N. Mårtensson, *Nature*, 2002, **418**, 620–623.

24 A. J. Britton, M. Weston and J. N. O'Shea, *Phys. Rev. Lett.*, 2012, **109**, 017401.

25 T. Schiros, G. Kladnik, D. Prezzi, A. Ferretti, G. Olivieri, A. Cossaro, L. Floreano, A. Verdini, C. Schenck, M. Cox, A. a. Gorodetsky, K. Plunkett, D. Delongchamp, C. Nuckolls, A. Morgante, D. Cvetko and I. Kymissis, *Advanced Energy Materials*, 2013, **3**, 894–902.

26 A. Batra, G. Kladnik, H. Vázquez, J. S. Meisner, L. Floreano, C. Nuckolls, D. Cvetko, A. Morgante and L. Venkataraman, *Nature Communications*, 2012, **3**, 1086.

27 P. Vilmercati, C. Castellarin-Cudia, R. Gebauer, P. Ghosh, S. Lizzit, L. Petaccia, C. Cepek, R. Larciprete, A. Verdini, L. Floreano, A. Morgante and A. Goldoni, *Journal of the American Chemical Society*, 2009, **131**, 644–652.

28 G. Kladnik, M. Puppin, M. Coreno, M. de Simone, L. Floreano, A. Verdini, A. Morgante, D. Cvetko and A. Cossaro, *Nano Letters*, 2016, **16**, 1955–1959.

29 P. Kao, S. Neppl, P. Feulner, D. L. Allara and M. Zharnikov, *The Journal of Physical Chemistry C*, 2010, **114**, 13766–13773.

30 D. Sánchez-Portal, D. Menzel and P. M. Echenique, *Physical Review B - Condensed Matter and Materials Physics*, 2007, **76**, 1–19.

31 D. Sánchez-Portal, *Progress in Surface Science*, 2007, **82**, 313–335.

32 G. Fratesi, C. Motta, M. I. Trioni, G. P. Brivio and D. Sánchez-Portal, *The Journal of Physical Chemistry C*, 2014, **118**, 8775–8782.

33 P. Persson, M. J. Lundqvist, R. Ernstorfer, W. A. Goddard and F. Willig, *Journal of Chemical Theory and Computation*, 2006, **2**, 441–451.

34 N. Martsinovich and A. Troisi, *The Journal of Physical Chemistry C*, 2011, **115**, 11781–11792.

35 T. Le Bahers, T. Pauporte, P. P. Laine, F. Labat, C. Adamo and I. Ciofini, *The Journal of Physical Chemistry Letters*, 2013, **4**, 1044–1050.

36 A. V. Akimov, A. J. Neukirch and O. V. Prezhdo, *Chemical Reviews*, 2013, **113**, 4496–4565.

37 M. Brandbyge, J.-L. Mozos, P. Ordejon, J. Taylor and K. Stokbro, *Physical Review B*, 2001, **65**, 18.

38 J. M. Soler, E. Artacho, J. D. Gale, A. Garcìa, J. Junquera, P. Ordejòn and D. Sànchez-Portal, *J. Phys.: Condens. Matter*, 2002, **14**, 2745–2779.

39 A. Nitzan and M. A. Ratner, *Science*, 2003, **300**, 1384–1389.

40 M. Hasegawa, K. Nishidate, T. Hosokai and N. Yoshimoto, *Physical Review B - Condensed Matter and Materials Physics*, 2013, **87**, 1–9.

41 G. Bertoni, L. Calmels, A. Altibelli and V. Serin, *Physical Review B - Condensed Matter and Materials Physics*, 2005, **71**, 1–8.

42 M. Fuentes-Cabrera, M. I. Baskes, A. V. Melechko and M. L. Simpson, *Physical Review B - Condensed Matter and Materials Physics*, 2008, **77**, 1–5.

43 A. Dahal and M. Batzill, *Nanoscale*, 2014, **6**, 2548.

44 A. Garcia-Lekue, T. Balashov, M. Olle, G. Ceballos, A. Arnau, P. Gambardella, D. Sánchez-Portal and A. Mugarza, *Physical Review Letters*, 2014, **112**, 066802.

45 F. Bianchini, L. L. Patera, M. Peressi, C. Africh and G. Comelli, *The Journal of Physical Chemistry Letters*, 2014, **5**, 467–473.

46 J. Klimeš, D. R. Bowler and A. Michaelides, *Journal of Physics: Condensed Matter*, 2010, **22**, 022201.

47 *Supplementary Info*.

48 L. Ould-Moussa, O. Poizat, M. Castella and M. Curie, *J. Phys. Chem.*, 1996, **100**, 2072–2082.

49 T. Susi, D. J. Mowbray, M. P. Ljungberg and P. Ayala, *Physical Review B - Condensed Matter and Materials Physics*, 2015, **91**, 1–5.

50 L. L. Patera, C. Africh, R. S. Weatherup, R. Blume, S. Bhardwaj, C. Castellarin-Cudia, A. Knop-Gericke, R. Schloegl, G. Comelli, S. Hofmann and C. Cepek, *ACS Nano*, 2013, **7**, 7901–7912.

51 Q. Wang, L. Wei, M. Sullivan, S.-W. Yang and Y. Chen, *RSC Advances*, 2013, **3**, 3046.

52 T. Abtew, B.-C. Shih, S. Banerjee and P. Zhang, *Nanoscale*, 2013, **5**, 1902.

53 P. Sutter, M. S. Hybertsen, J. T. Sadowski and E. Sutter, *Nano Letters*, 2009, **9**, 2654–2660.

54 A. Varykhalov, J. Sánchez-Barriga, A. M. Shikin, C. Biswas, E. Vescovo, A. Rybkin, D. Marchenko and O. Rader, *Physical Review Letters*, 2008, **101**, year.

55 C. Africh, C. Cepek, L. L. Patera, G. Zamborlini, P. Genoni, T. O. Mentes, A. Sala, A. Locatelli and G. Comelli, *Scientific Reports*, 2016, **6**, year.

56 J. Ben Taylor, L. C. Mayor, J. C. Swarbrick, J. N. O'Shea, C. Isvoranu and J. Schnadt, *The Journal of Chemical Physics*, 2007, **127**, 134707.

57 S. Lizzit, R. Larciprete, P. Lacovig, K. L. Kostov and D. Menzel, *ACS Nano*, 2013, **7**, 4359–4366.

58 A. Ravikumar, A. Baby, H. Lin, G. P. Brivio and G. Fratesi, *Scientific reports*, 2016, **6**, 24603.

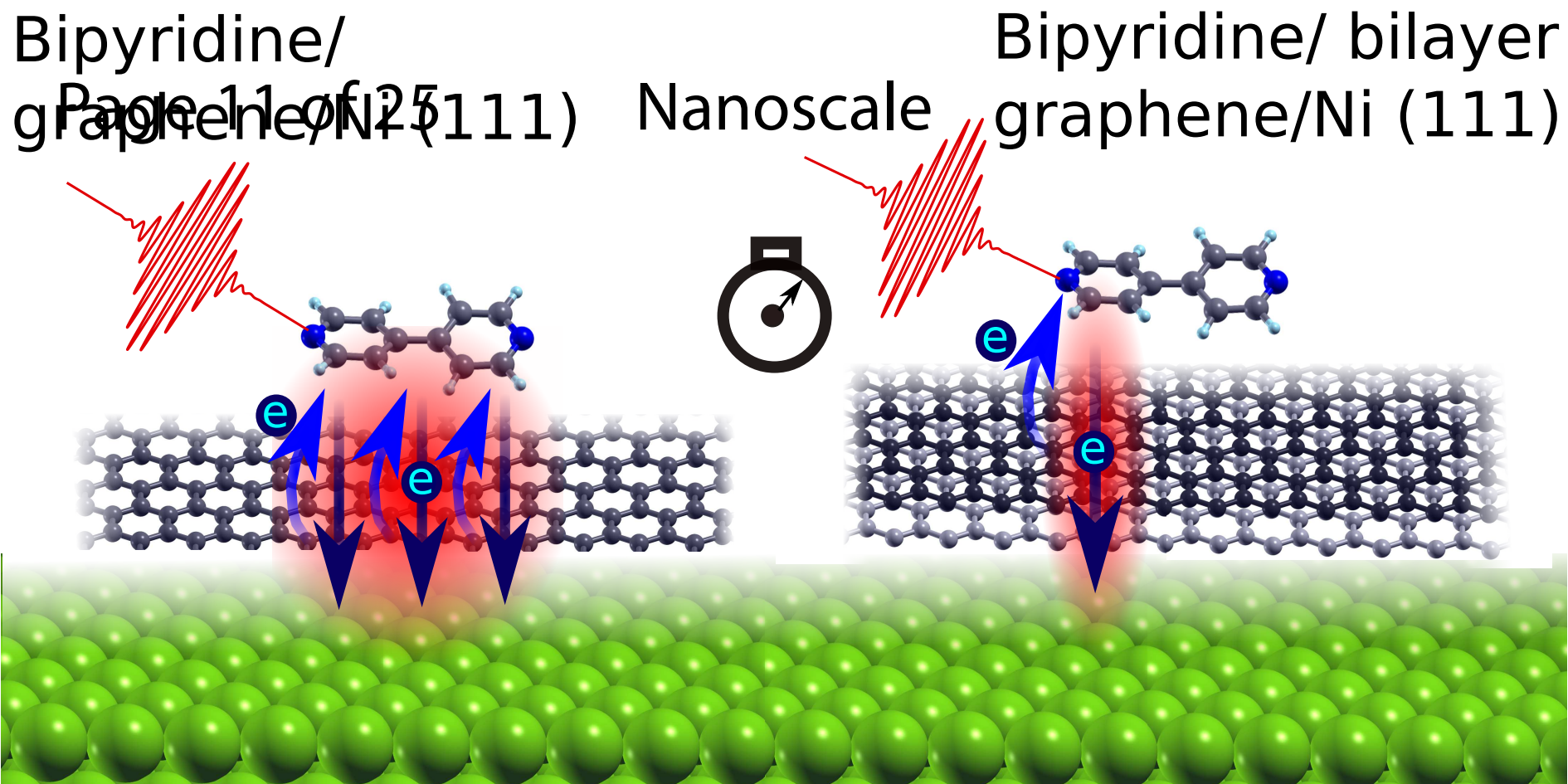
Bipyridine/
graphene/Ni (111)
e
e
Bipyridine/ bilayer
graphene/Ni (111)
e
e

Supporting Information for Substrate induced ultrafast electron injection dynamics of organic-graphene interface

Abhilash Ravikumar[1], Gregor Kladnik[2,3], Moritz Müller[4], Albano Cossaro[5], Gregor Bavdek[6], Laerte L. Patera[3,5], Daniel Sánchez Portal [4], Latha Venkataraman[7,8], Alberto Morgante[3,5], Gian Paolo Brivio[1], Dean Cvetko[2,5,9] and Guido Fratesi[10]

[1] *Università di Milano-Bicocca,Via Cozzi 55 - 20125 Milano, Italy.*

[2] *Faculty for mathematics and physics, University of Ljubljana, Slovenia*

[3] *Dipartimento di Fisica, Università di Trieste, Italy*

[4] *entro de Física de Materiales, Paseo Manuel de Lardizabal 5, 20018 San Sebastián, Spain*

[5] *CNR-IOM Laboratorio Nazionale TASC, Trieste, Italy*

[6] *Faculty of education, University of Ljubljana, Ljubljana, Slovenia*

[7] *Dept. of Applied Physics and Applied Mathematics, Columbia University, New York*

[8] *Dept. of Chemistry, Columbia University, New York*

[9] *Institut J. Stefan, Janova 39, Ljubljana, Slovenia*

[10] *Dipartimento di Fisica, Università degli Studi di Milano, Via Celoria, 16 - 20133 Milano, Italy*

---

1 Additional information concerning the simulations

Structural optimization of bipyridine on free-standing graphene

To address the various adsorption configurations of bipyridine on pristine, free-standing graphene (FSG) we extended to this molecule our previous investigation of pyridine and related radicals on graphene[1]. Accordingly, we make use of the ab initio density functional theory (DFT) simulation platform Quantum Espresso [2] that uses pseudopotentials and plane-wave basis set. The system

is setup within Generalized Gradient Approximation using Perdew-Burke-Ernzerholf (PBE) exchange correlational functional [3, 4] and the Grimme correction is used to take into account non-local van der Waals interaction [5]. Bipyridine is adsorbed on a 5×7 graphene supercell periodic in the *xy* plane and a vacuum separation of 15 Å of periodically repeated systems in the *z* direction. The plane wave kinetic energy cut-off is 42 Ry and the convergence on the energy and force are 10^{-4} a.u. and 10^{-3} a.u., respectively. The surface Brillouin zone is sampled using a 15×14 Γ-centered **k** grid for calculating the system energy and a 18×12 Γ centered grid for the density of states (DOS) calculations (the latter corresponding to a 90×84 grid in the 1×1 unit cell). We considered the configurations shown in Fig. S1, whose energies and structural parameters are summarized in Table 1. The CT-armchair configuration was found to be the most stable, although a mild dependence of the adsorption energy points to high molecular diffusivity and possible coexistence of different adsorption sites. The optimized coordinates of CT-armchair have been chosen as the starting point for the later SIESTA/TranSIESTA structural optimizations and the calculations of the DOS, that instead adopt a localized basis sets (see the main text). We checked the equivalence of the computed DOS of BP/FSG in the ground and excited states by the two approaches.

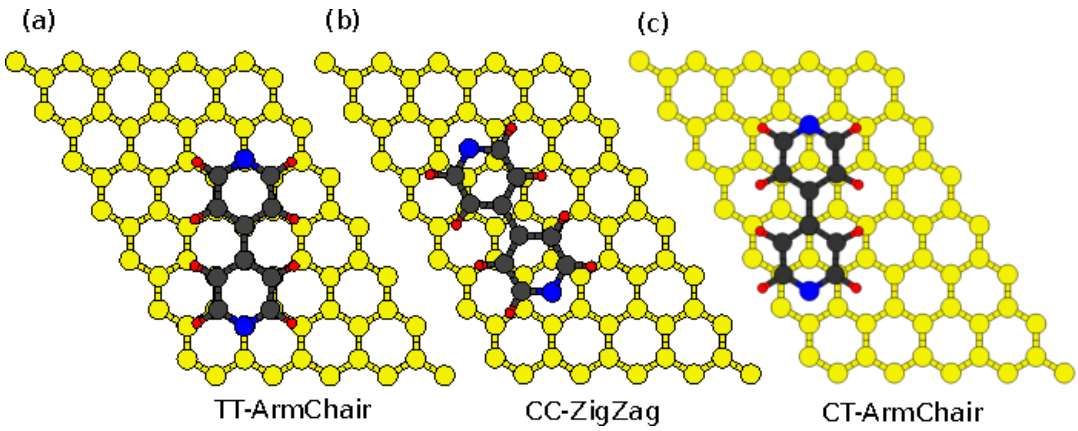

Figure S1: The configurations of bipyridine on graphene which were studied are (a) TT-ArmChair : where the nitrogen atoms of the molecule are on top of the carbon atoms of the graphene ring and the in-plane axis connecting these nitrogen atoms pass above armchair graphene. (b) CC-ZigZag: the nitrogen atoms of the molecule are on the center of a graphene ring with the in-plane axis passing above zigzag graphene. (c) CT-ArmChair: where the nitrogen atoms are on top of a graphene atom and in the center of the graphene ring.

Configuration	E_{ads} (meV)	$a_{BP\text{-}G}$ Å	Torsional angle (θ°)
TT-ArmChair	-679	3.34	9.7
CC-ZigZag	-752	3.23	9.5
CT-ArmChair	-782	3.09	9.2

Table 1: The adsorption energies (E_{ads}), Bipyridine-graphene equilibrium bond distance ($a_{BP\text{-}G}$) and Bipyridine torsional angle (θ) after adsorption is tabulated for these configurations with Grimme correction. Gas phase bipyridine torsional angle is reported to be 37°[6].

Molecular break junction setup

The now describe the break junction setup employed for our calculations of molecules adsorbed on a semi-infinite substrate. We model a semi-infinite substrate to better describe a bulk continuum as shown in Fig. S2. We utilize the Green's function formalism within DFT to deal with such systems. The system is setup as a 6×6 surface supercell with two semi infinite electrode regions and a central scattering one. The electrodes are composed of three Ni layers on either side. The central scattering region consists of bipyridine adsorbed on epitaxial graphene/nickel and bilayer graphene/nickel substrates as shown in Fig. 1(b) and (c) of the main article. With respect to our previous work and in order to reduce the number of atoms involved in the calculation, an asymmetric break-junction setup is used at variance than in our previous calculations [7, 8]. The system is periodic in the *xy* direction and a vacuum separation of 35 Å is used along the transport direction *z* to ensure minimal interaction between the periodic images and an almost constant electrostatic potential between the asymmetric leads.

The density of states $\rho_\phi(E)$ projected on the molecular orbital ϕ of interest (PDOS) is then fitted by a Lorentzian function to extract the linewidth. Since we are interested in the resonant lifetime for an initially localized state, rather than for one with definite momentum, the evaluation of ρ_ϕ includes an integral over the surface Brillouin zone [7]. However, we could check that in this specific case (LUMO of BP in BP/EG/Ni and BP/BLG/Ni) the contributions to the PDOS at zone center and zone boundary superimpose, so the BZ sampling could be restricted to a coarser mesh

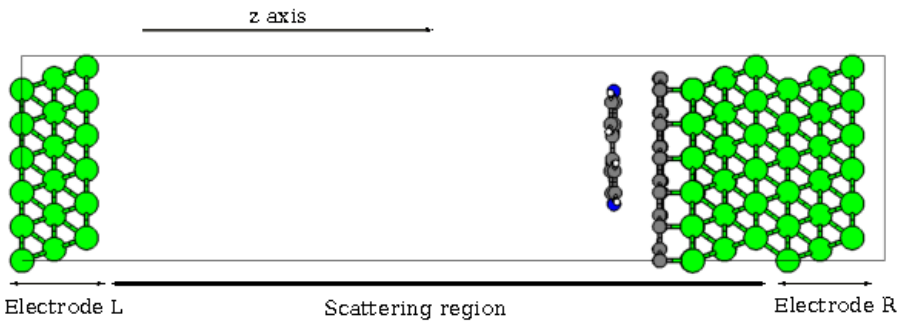

Figure S2: The break junction setup shows three layers of Ni as electrodes on either sides which are coupled to bulk continuum by self energy operators. The central scattering region is asymmetric with the molecule adsorbed on one side and the two regions are decoupled by a large vacuum separation of 35 Å.

(equivalent to a 12×12 one for clean Ni(111)) than for the self-consistent calculations.

Gas phase molecular orbitals of bipyridine

Frontier gas phase molecular orbitals of bipyridine are plotted for reference in Fig. S3. We recall that our analysis focuses on the LUMO so that the relative alignment of the other orbitals (especially of σ with respect to π states, given they suffer differently from self-interaction errors[9]) is not relevant for our results. We mention on this respect that by an additional calculation with an hybrid functional (PBE0)[10] we reproduced the same ordering as reported here.

Density of states for ground state and core-excited adsorbed bipyridine

We report here a detailed decomposition of the DOS for the three systems we have studied.

Figure S4 summarizes the DOS of BP/EG/Ni. The total DOS, and its projections on the top and bottom layers of graphene are shown. Details regarding the DOS are discussed in detail in the

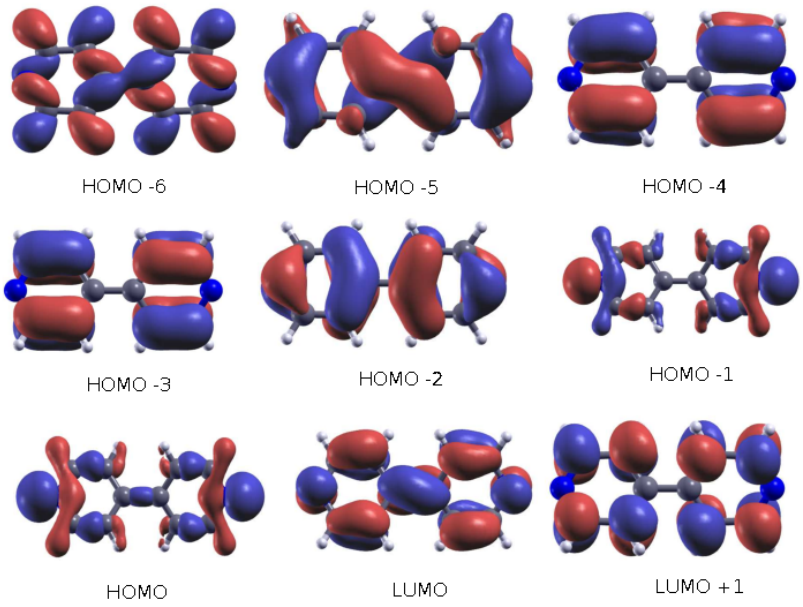

Figure S3: Gas phase molecular orbitals of bipyridine.

main text. We also repeat for convenience the projections onto the molecular orbitals of bipyridine in the ground and core excited state.

Figure S5 summarizes the same quantities for BP/BLG/Ni. Here in addition to the total DOS, its projections on the top and bottom layers of graphene are shown separately.

We also plot the ground and core excited state DOS of BP/FSG as shown in Fig. S6.

Resonant coupling for spin-minority LUMO* states

We now detail the procedure employed to evaluate the charge transfer time for the spin-minority LUMO*. In our spin-collinear electronic structure relaxation, the valence electronic density in the two spin populations is determined self-consistently without any constraint. This resulted in the spin-majority bipyridine state being populated upon the excitation, which represents the electronic ground state (with a N1s atom). In the experiments, resonant core-excitation to the LUMO* state could however equally involve a spin-minority electron. To model this case, that could be though as an inversion of the molecular spin density also given that the electrostatic interaction with the core

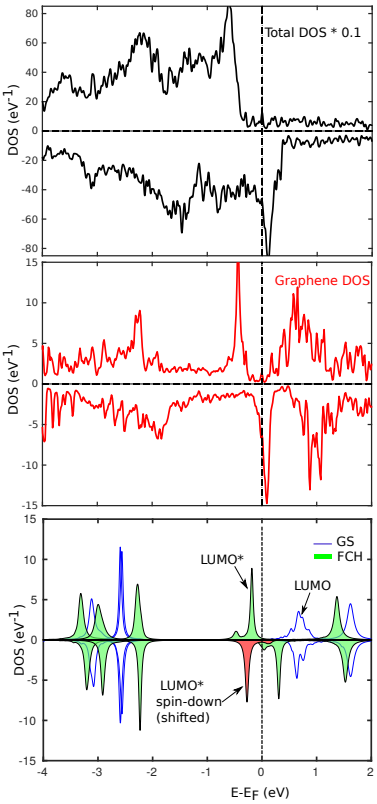

Figure S4: The total DOS of BP/EG/Ni, and its projections on the graphene layer are shown. The projections onto the molecular orbitals in the ground state (GS) and in the core excited one (FCH) are also plotted.

is the main perturbation to the energy levels of the free molecule, we therefore need to consider a spin-minority LUMO* at about the same energy below the Fermi level, as the spin-majority one computed self-consistently. This is achieved here by applying as a post-self-consistent correction a shift of the Hamiltonian matrix elements belonging to the molecule, a procedure implemented and tested in our previous work:[7]

$$H_{\mu\nu\mathbf{k}_\parallel} = H_{\mu\nu\mathbf{k}_\parallel} + S_{\mu\nu\mathbf{k}_\parallel}\Delta\varepsilon, \quad \mu,\nu \in \text{molecule}. \tag{1}$$

In the above, S is the overlap operator and $\mu,\nu,\mathbf{k}_\parallel$ stand for the localized basis set indexes and the surface wavevector. By a shift of $\Delta\varepsilon = -0.5$ eV we effectively align the spin-minority LUMO* peak position in the DOS (for example in BP/EG/Ni) to the desired value below the Fermi energy,

as shown in Fig. S4 and Fig. S5 for BP/EG/Ni(111) and BP/BLG/Ni(111), respectively. Then we evaluate its resonant fwhm as a result of coupling with spin-minority Ni states.

Work function for EG/Ni(111) and BLG/Ni(111)

The adsorption of graphene on Ni(111) modifies the electrostatic dipole and hence the work function of the substrate, Φ. Our calculations performed for the (1×1) unit cell of EG/Ni(111) (without adsorbed molecules) produced a decrease of Φ by 1.0 eV with respect to the one of clean Ni(111), in agreement to the literature[11] (see Fig. S7). In the case of BLG/Ni(111), Φ is instead reduced by only 0.3 eV, so that the addition of a second layer of graphene over EG/Ni(111) produces an increase of Φ by 0.7 eV. (We notice that an even larger increase of the work function when passing from single to bilayer graphene, 1.0 eV, has been found for a Ru(0001) substrate[12].) This variation is consistent with a similar shift away from the Fermi energy, when passing from BP/EG/Ni to BP/BLG/Ni, that can be appreciated for the BP molecular orbitals in Fig. 2 of the main text.

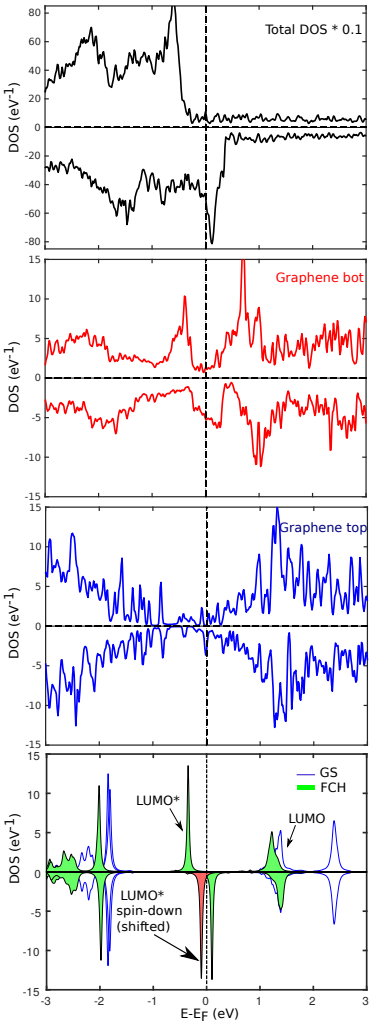

Figure S5: The total DOS of BP/BLG/Ni, and its projections on the bottom and on the top graphene layer are shown. The projections onto the molecular orbitals in the ground state (GS) and in the core excited one (FCH) are also plotted.

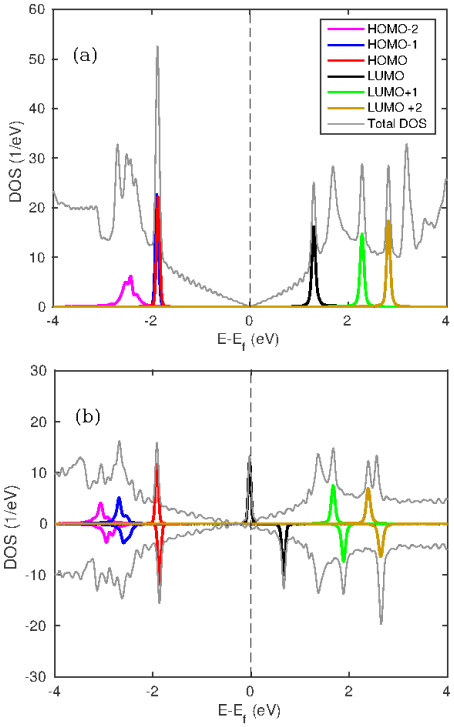

Figure S6: The total DOS of BP/FSG/Ni, its projections onto the molecular orbitals in (a) the ground state and (b) the core excited state are shown.

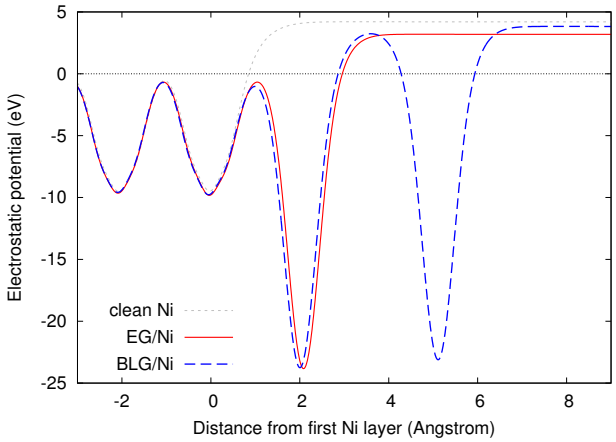

Figure S7: Electrostatic potentials for clean Ni(111), EG/Ni(111), and BLG/Ni(111). Results are averaged over planes parallel to the surface and shown with reference to the Fermi energy.

2 Additional information concerning the experiments

Synthesis of EG and BLG phases of graphene

The synthesis of EG and BLG phases on Ni(111) has been performed in-situ, by ethylene adsorption in 10^{-6} mbar atmosphere on Ni(111) held at 400°C (650°C). The quality of the EG (BLG) phase was monitored by UV photoemission with 40.8 eV photon energy where characteristic π band at Γ at 10.5 eV (8.5 eV) binding energy was evidenced accompanied by adequate attenuation of the Ni3*d* band features, in agreement with preparation procedures reported by Patera et al.[13]. For both phases EG and BLG, carbon 1*s* XPS was regularly checked with characteristic peaks detected at 285 eV (284.5 eV) binding energy.

NEXAFS measurements

Experimental observations of the molecular geometry are studied using Nitrogen 1*s* Near Edge X-ray Absorption Fine Structure (NEXAFS) which is shown in Fig. S8. The NEXAFS for both the systems show a very similar electronic structure the empty bipyridine orbitals. The main peak corresponds to the N1*s* $\rightarrow$LUMO transition. The LUMO of BP has a π character with the nodal plane coinciding with the molecular aromatic ring. The NEXAFS spectra were recorded with photon electric field $\vec{\varepsilon}$ aligned along the substrate normal (p-pol) and with $\vec{\varepsilon}$ lying in the surface plane (s-pol). For BP multilayer the intensity of the LUMO excitation is independent of the electric field polarization, as can be expected for a randomly oriented molecular film. BP/EG/Ni and BP/BLG/Ni monolayer films, on the contrary, display a very strong and almost identical linear dichroism which suggests an almost flat lying adsorption geometry of the molecule. From the π peak intensity analysis we find BP molecular long axis almost parallel to the substrate with average inclination of the BP phenyl rings of 16° and $20° \pm 3°$, for BP/EG/Ni and BP/BLG/Ni, respectively which are in close agreement with theoretically calculated angles.

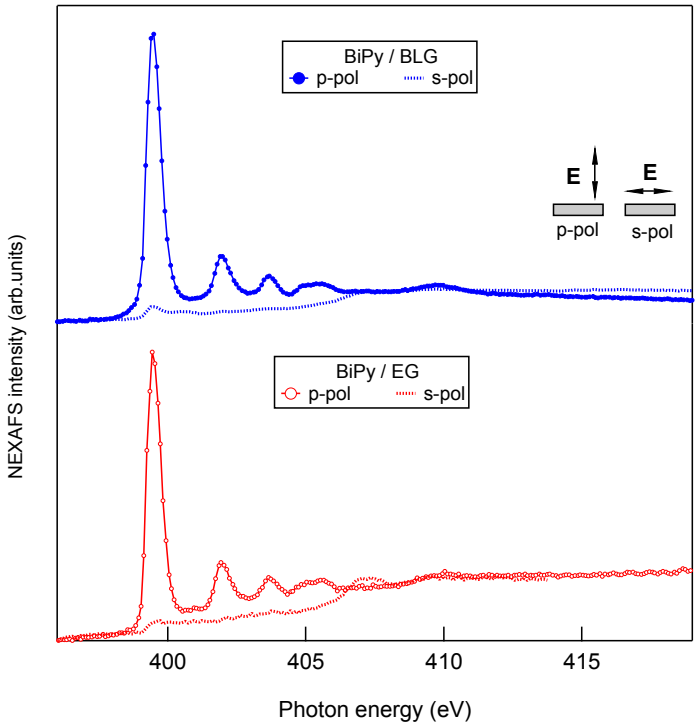

Figure S8: NEXAFS spectra in p-polarization (line with markers) and s-polarization (dashed lines) for BP/EG/Ni (red color, lower panel) and BP/BLG/Ni (blue color, upper panel). The direction of the photon field in the two polarizations is depicted in the inset.

Valence band photoemission

UV valence band photoemission experiments were performed at HASPES /ALOISA beamline with He discharge source using of 40.8 eV from He II line. Angle resolved spectra were collected with a 150 mm hemispherical electron analyzer with 2° acceptance angle, by rotating the sample polar angle in steps of 2° . The overall energy resolution was 0.1 eV. The Ni(111) and EG phase the surface orientation was aligned by rotating sample azimuthal orientation (around surface normal) which allowed us to collect angle resolved spectra along ΓK and ΓM surface directions. For BLG phase there was no azimuthal dependence in the spectra due to polydispersion of azimuthally equivalent domains.

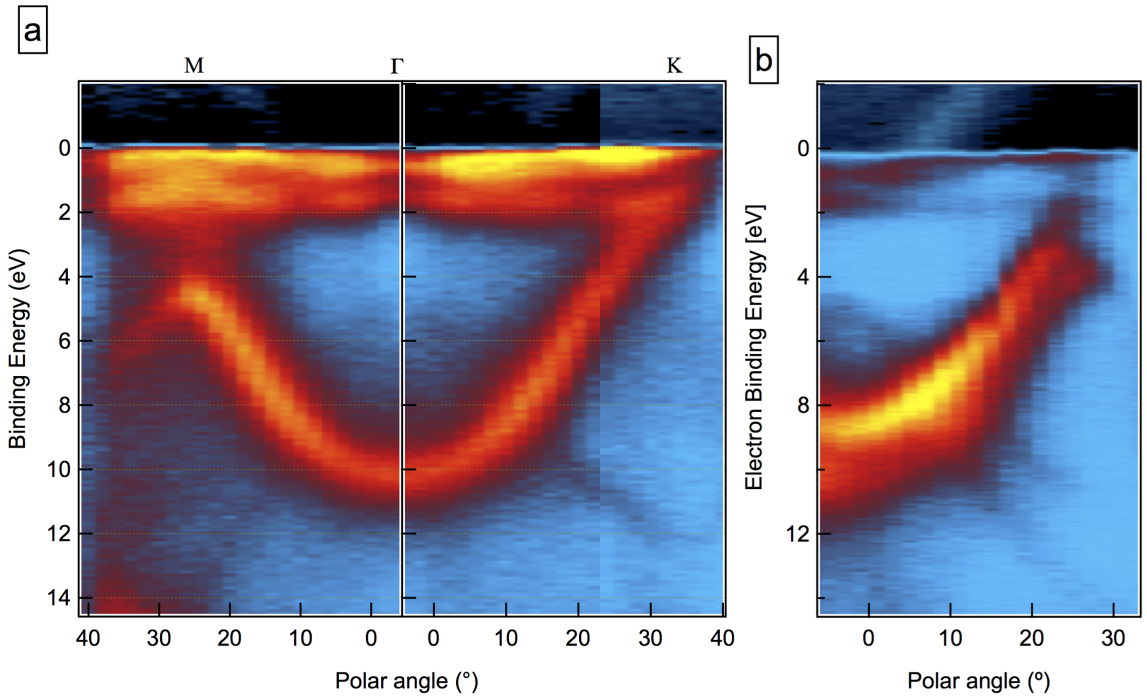

Figure S9: (a) EG phase ARUPS with photon energy of 40.8 eV (He II line) along ΓM and ΓK surface direction, showing the GR π band dispersion with band bottom at Γ reaching −10.5 eV. (b) BLG phase ARUPS with GR band bottom at Γ reaching −8.5 eV, consistent with the electronic structure of poorly interacting topmost GR layer. Some residual of the EG layer beneath may also be observed in the spectrum.

References

[1] A. Ravikumar, A. Baby, H. Lin, G. P. Brivio, and G. Fratesi, "Femtomagnetism in graphene induced by core level excitation of organic adsorbates.," *Scientific reports*, vol. 6, no. April, p. 24603, 2016.

[2] P. Giannozzi, S. Baroni, N. Bonini, M. Calandra, R. Car, C. Cavazzoni, D. Ceresoli, G. L. Chiarotti, M. Cococcioni, I. Dabo, A. Dal Corso, S. de Gironcoli, S. Fabris, G. Fratesi, R. Gebauer, U. Gerstmann, C. Gougoussis, A. Kokalj, M. Lazzeri, L. Martin-Samos, N. Marzari, F. Mauri, R. Mazzarello, S. Paolini, A. Pasquarello, L. Paulatto, C. Sbraccia, S. Scandolo, G. Sclauzero, A. P. Seitsonen, A. Smogunov, P. Umari, and R. M. Wentzcovitch, "QUANTUM ESPRESSO: a modular and open-source software project for quantum

simulations of materials.," *Journal of physics. Condensed matter : an Institute of Physics journal*, vol. 21, p. 395502, sep 2009.

[3] J. Perdew, K. Burke, and Y. Wang, "Generalized gradient approximation for the exchange-correlation hole of a many-electron system," *Physical Review B*, vol. 54, pp. 16533–16539, dec 1996.

[4] J. Perdew, K. Burke, and M. Ernzerhof, "Generalized Gradient Approximation Made Simple.," *Physical Review Letters*, vol. 77, pp. 3865–3868, oct 1996.

[5] S. Grimme, "Semiempirical GGA-type density functional constructed with a long-range dispersion correction," *Journal of Computational Chemistry*, vol. 27, pp. 1787–1799, nov 2006.

[6] L. Ould-Moussa, O. Poizat, M. Castella, and M. Curie, "Ab Initio Computations of the Geometrical, Electronic, and Vibrational Properties of the Ground State, the Anion Radical, and the N,N'-Dihydro Cation Radical of 4,4'-Bipyridine Compared to Transient Raman Spectra," *J. Phys. Chem.*, vol. 100, pp. 2072–2082, 1996.

[7] G. Fratesi, C. Motta, M. I. Trioni, G. P. Brivio, and D. Sánchez-Portal, "Resonant Lifetime of Core-Excited Organic Adsorbates from First Principles," *The Journal of Physical Chemistry C*, vol. 118, pp. 8775–8782, may 2014.

[8] D. Cvetko, G. Fratesi, G. Kladnik, A. Cossaro, G. P. Brivio, L. Venkataraman, and A. Morgante, "Ultrafast electron injection into photo-excited organic molecules," *Phys. Chem. Chem. Phys.*, vol. 18, no. 32, pp. 22140–22145, 2016.

[9] S. Refaely-Abramson, S. Sharifzadeh, N. Govind, J. Autschbach, J. B. Neaton, R. Baer, and L. Kronik, "Quasiparticle spectra from a nonempirical optimally tuned range-separated hybrid density functional," *Physical Review Letters*, vol. 109, p. 226405, Nov 2012.

[10] C. Adamo and V. Barone, "Toward reliable density functional methods without adjustable parameters: The pbe0 model," *The Journal of Chemical Physics*, vol. 110, no. 13, p. 6158, 1999.

[11] R. Rosei, S. Modesti, F. Sette, C. Quaresima, A. Savoia, and P. Perfetti, "Electronic structure of carbidic and graphitic carbon on Ni(111)," *Physical Review B*, vol. 29, pp. 3416–3422, Mar. 1984.

[12] P. Sutter, M. S. Hybertsen, J. T. Sadowski, and E. Sutter, "Electronic Structure of Few-Layer Epitaxial Graphene on Ru(0001)," *Nano Letters*, vol. 9, pp. 2654–2660, July 2009.

[13] L. L. Patera, C. Africh, R. S. Weatherup, R. Blume, S. Bhardwaj, C. Castellarin-Cudia, A. Knop-Gericke, R. Schloegl, G. Comelli, S. Hofmann, and C. Cepek, "*In Situ* Observations of the Atomistic Mechanisms of Ni Catalyzed Low Temperature Graphene Growth," *ACS Nano*, vol. 7, pp. 7901–7912, Sept. 2013.